The Journal of Chemical Physics

Photodissociation of CH_2. III. Two-dimensional dynamics of the dissociation of CH_2, CD_2, and CHD through the first excited triplet state

Cite as: J. Chem. Phys. **100**, 1113 (1994); https://doi.org/10.1063/1.466643
Submitted: 26 May 1993 . Accepted: 19 October 1993 . Published Online: 31 August 1998

Robert A. Beärda, Geert-Jan Kroes, Marc C. van Hemert, Bernd Heumann, Reinhard Schinke, and Ewine F. van Dishoeck

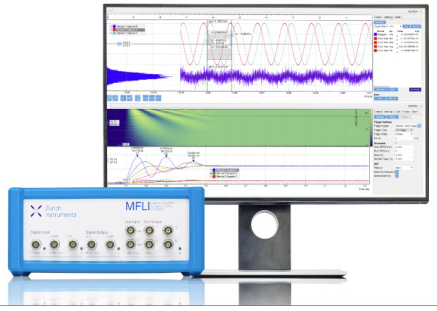

Photodissociation of CH_2. III. Two-dimensional dynamics of the dissociation of CH_2, CD_2, and CHD through the first excited triplet state

Robert A. Beärda, Geert-Jan Kroes, and Marc C. van Hemert
Gorlaeus Laboratories, P.O. Box 9502, 2300 RA Leiden, The Netherlands

Bernd Heumann and Reinhard Schinke
Max-Planck-Institut für Strömungsforschung, Bunsenstrasse 10, D-3400, Göttingen, Germany

Ewine F. van Dishoeck
Sterrewacht Leiden, P.O. Box 9513, 2300 RA Leiden, The Netherlands

(Received 26 May 1993; accepted 19 October 1993)

We present quantitative results on photodissociation of CH_2 ($\tilde{X}\,^3B_1$) and its isotopomers CHD and CD_2 through the first excited triplet state ($1\,^3A_1$). A two-dimensional wave packet method employing the light–heavy–light approximation was used to perform the dynamics. The potential energy surfaces and the transition dipole moment function used were all taken from *ab initio* calculations. The peak positions in the calculated CH_2 and CD_2 spectra nearly coincide with the positions of unassigned peaks in experimental CH_2 and CD_2 $3+1$ resonance enhanced multiphoton ionization spectra, provided that the experimental peaks are interpreted as two-photon transitions. Comparing the photodissociation of CH_2 and its isotopomers to photodissociation of water in the first absorption band, we find these processes to be very similar in all aspects discussed in this work. These aspects include the origin of the diffuse structure and the overall shape of the total absorption spectra of vibrationless and vibrationally excited CH_2, trends seen in the fragment vibrational level distribution of the different isotopomers, and selectivity of photodissociation of both vibrationless and vibrationally excited CHD. In particular, we find that the CD/CH branching ratio exceeds two for all wavelengths in photodissociation of vibrationless CHD.

I. INTRODUCTION

In the interstellar medium, photodissociation is one of the most important processes for the destruction of molecules. A molecule that is of considerable astrophysical interest is methylene (CH_2).[1,2] Unfortunately, to the best of our knowledge there is no experimental information concerning photodissociation of $\tilde{X}\,^3B_1$ CH_2 through its lower-line triplet states, although *ab initio* calculations[3] have predicted that photodissociation should occur effectively through its lowest excited triplet state, the $1\,^3A_1$ state. In this paper results will be presented on photodissociation of CH_2 into CH ($X\,^2\Pi$) + H(^2S) through this state. It is our hope that the results presented here, which can be used for astrophysical modeling, will also be of help to experimentalists in finding the transition to the lowest excited triplet state.

In two previous papers,[4,5] we reported results of calculations aimed at obtaining quantitative cross sections for the photodissociation of CH_2. In the first paper,[4] we discussed two-dimensional *ab initio* potential energy surfaces for the ground state and for nine excited triplet states. In the second paper,[5] full three-dimensional potential energy surfaces were presented for the $\tilde{X}\,^3B_1$ ground state and the lowest excited triplet state. Subsequently, these surfaces were used for performing three-dimensional wave packet calculations on the $1\,^3A_1 \leftarrow \tilde{X}\,^3B_1$ transition.

From our potential surface studies,[4] it stands clear that at low photon energies, 5.7–9.2 eV, CH_2 can dissociate into CH + H through its first two excited triplet states, the $1\,^3A_1$ and the coupled $1\,^3A_2/2\,^3B_1$ states. Through the second excited triplet state, dissociation into C and H_2 is also possible and proceeds without a barrier. This last aspect makes photodissociation from CH_2 different from the most studied case, water,[6–12] where dissociation into $O(^1D)+H_2$ through the first excited state ($^1B_1$) is impeded by a barrier of 0.4 eV, while there is no barrier for dissociation into OH and H through the same state.[13] For photodissociation of CH_2 through the second excited triplet state therefore not only cross sections in the individual channels are needed, but also branching ratios. In this work we do not present any results on photodissociation through the $1\,^3A_2$ state, but instead focus on photodissociation through the $1\,^3A_1$ state, into CH + H.

Our three-dimensional dynamics studies[5] on the $1\,^3A_1 \leftarrow \tilde{X}\,^3B_1$ transition presented both total and partial (vibrational and rotational) cross sections. A comparison of the absorption spectrum with results of two-dimensional wave packet calculations (in which the bending angle was kept fixed at its ground state equilibrium value) showed that a two-dimensional treatment suffices for obtaining accurate total cross sections, as is the case for photodissociation of water through its first excited state.[14] Similarly, the vibrational level distribution in the fragment obtained from two-dimensional calculations compared well with the three-dimensional results.[15] In contrast, a three-dimensional treatment is necessary for obtaining correct final rotational state distributions. The reason for this is that the excited state potential shows considerable anisotropy in the exit channel. In the Franck-Condon region, the dependence of the excited state potential on the bending

 0021-9606/94/100(2)/1113/15/$6.00

coordinate is much weaker, which explains why the bending mode may be neglected in calculating total and vibrationally resolved cross sections.

In addition to yielding accurate results for photodissociation of methylene, the two-dimensional method is much less time consuming than the three-dimensional wave packet method. We have therefore used the two-dimensional method to also obtain cross sections for photodissociation of CHD and CD_2, and to explore the photodissociation of vibrationally excited CH_2 and CHD. An interesting aspect of photodissociation of CHD is whether there is a preference for the production of CH or CD. Calculations[16,17] on initially vibrationless HOD have predicted a clear preference for the production of OD, which has been confirmed experimentally.[18] Excitation of the OH stretch prior to dissociation was predicted[16,17] to lead to enhanced OD/OH branching ratios for most UV wavelengths, which was also confirmed experimentally.[19–22]

Photodissociation from excited vibrational states of the parent molecule is of interest because larger parts of the potential energy surfaces are sampled. As was shown for water, photodissociation from states where the symmetric stretch is excited differs widely from that starting from a state in which the antisymmetric stretch is excited.[7,9] Further, selective initial vibrational excitation might be advantageous in experimental CH_2 photodissociation studies. In these experiments, the production of CH_2 molecules in the $^3B_1$ ground state is accompanied by the production of CH_2 in singlet states and other carbonhydrides[23] which have different vibrational frequencies. Perhaps selective vibrational excitation of CH_2 prior to dissociation will diminish the interference (e.g., by unwanted CH fragments) of these other molecules.

In many experimental photodissociation studies of triatomic molecules, the final state distribution of the fragment is probed, e.g., using laser induced fluorescence. For this reason, in most cases we also present cross sections that are resolved with respect to the final vibrational state of the fragment.

In a previous paper,[5] we already stressed that astrophysical models require quantitative cross sections (in absolute units, not arbitrary units). In this paper, we rederive the relation of Untch *et al.*[24] (originally due to Kulander and Heller)[25] for calculating partial cross sections, this time obtaining an exact expression.

With the photodissociation of CH_2 we have what is perhaps a rather unique situation for photodissociation of triatomics: at present, theory is ahead in making predictions. It is our hope that the results presented here will set off experiments designed to test the predictions made in this work and give validity to our approach.

II. METHODS

A. Dynamics

In a time-dependent formalism, the total photodissociation cross section can be expressed in Système International (SI) units as[26–28]

$$\sigma(E)=\frac{\pi\nu}{3c\epsilon_0\hbar}\int_{t=-\infty}^{t=\infty} e^{iEt/\hbar}\langle\Phi(\mathbf{Q},t=0)\,|\,\Phi(\mathbf{Q},t)\rangle dt \tag{1}$$

with

$$\Phi(\mathbf{Q},t=0)=\mu(\mathbf{Q})\Psi_i(\mathbf{Q}). \tag{2}$$

In these equations, $\mathbf{Q}$ is the set of nuclear coordinates. In our two-dimensional approach, this set consists of the two C–H bond lengths, r_1 and r_2. The total energy E is $E_i+h\nu$, in which ν is the frequency of the exciting radiation and E_i is the initial vibronic energy of methylene. The initial and final electronic states are connected by the transition dipole moment function $\mu(r_1,r_2)$, and $\Psi_i(r_1,r_2)$ is the nuclear wave function of the molecule in its initial electronic state with corresponding vibronic energy E_i. The propagated wave function $\Phi(r_1,r_2,t)$ is obtained as $e^{-i\hat{H}t/\hbar}\Phi(r_1,r_2,t=0)$ using the Hamiltonian for nuclear motion, which, in the light–heavy–light (LHL) approximation, is taken as

$$\hat{H}=\frac{-\hbar^2}{2m_1}\frac{\partial^2}{\partial r_1^2}-\frac{\hbar^2}{2m_2}\frac{\partial^2}{\partial r_2^2}+V_{\mathrm{el}}(r_1,r_2;\alpha_{\mathrm{eq}}), \tag{3}$$

where $V_{\mathrm{el}}(r_1,r_2;\alpha_{\mathrm{eq}})$ is the appropriate excited electronic state potential energy surface as a function of both r_1 and r_2 at a fixed value of the bond angle (α_{eq} is the equilibrium angle in the electronic ground state). In this equation, m_1 and m_2 are the reduced masses of the corresponding CH fragment. The overlap integral $\langle\Phi(r_1,r_2,t=0)\,|\,\Phi(r_1,r_2,t)\rangle$ is referred to as the autocorrelation function. Note that this autocorrelation function will usually differ from unity at $t=0$, due to the inclusion of the transition dipole moment function.

In writing Eq. (3), we have neglected the kinetic term which couples the CH oscillators. In calculations on the photodissociation of water, it was found that the inclusion of this term leads to only very small changes in the photodissociation dynamics.[29] The prefactor $\cos\alpha/m_c$ (m_c is the mass of the central atom) occurring in the coupling term is much higher for CH_2 than for H_2O mainly because the ground state equilibrium angle of CH_2 is much larger. We have therefore tested to what extent the inclusion of the coupling term affects the photodissociation of CH_2. Because only small changes (1%–2%) of the total cross section for photodissociation of CH_2 were found, we concluded that it was safe to neglect the coupling term.

In calculations on the Raman emission spectrum of photodissociating molecules[29,30] and in calculations on photodissociation of initially highly excited stretching states, the kinetic coupling term should be included. This is because for vibrational states containing two or more stretching quanta, the kinetic coupling affects the degree of mixing of wave functions with the same number of stretching quanta and symmetry (i.e., the extent to which the wave functions are normal modelike or local modelike).[31,32]

To calculate vibrationally resolved cross sections, Untch *et al.*[24] have derived the relation

$$\sigma_v(E) \sim \omega \frac{m_1}{k_v(E)} \lim_{t\to\infty} |A_v[k_v(E),t]|^2 \tag{4}$$

in which $A_v[k_v(E),t]$ is the wave function in momentum space describing the translational motion of the CH fragment in the vibrational state v and

$$k_v(E) = \frac{\sqrt{2m_1(E-E_v)}}{\hbar}, \tag{5}$$

where E_v is the vibronic energy of the fragment state labeled by v. Here, we derive the corresponding expression appropriate for calculating cross sections in absolute units.

In the standard time-independent formalism, the partial cross sections for formation of a vibrationally excited fragment with quantum number v can be expressed in SI units as[27,28,33]

$$\sigma_v(E) = \frac{\pi\omega}{3c\epsilon_0} |\langle \psi_v^-(r_1,r_2,E)|\mu(r_1,r_2)|\Psi_i(r_1,r_2)\rangle|^2 \tag{6}$$

in which the integration is performed over r_1 and r_2. The scattering wave function $\psi_v^-(r_1,r_2,E)$ corresponds asymptotically to an outgoing wave in the fragment channel v and is normalized on the energy scale. The link between the time-independent expression (6) and the appropriate time-dependent formula can be made by realizing that the absolute value of the overlap between $\Phi(r_1,r_2,t)$ and $\psi_v^-(r_1,r_2,E)$ is time independent, so that

$$|\langle \psi_v^-(r_1,r_2,E)|\Phi(r_1,r_2,t=0)\rangle| = |\langle \psi_v^-(r_1,r_2,E)|\Phi(r_1,r_2,t)\rangle|. \tag{7}$$

Therefore,

$$\sigma_v(E) = \frac{\pi\omega}{3c\epsilon_0} |\langle \psi_v^-(r_1,r_2,E)|\Phi(r_1,r_2,t)\rangle|^2 \tag{8}$$

is valid for all times t. The scattering wave function may be approximated at $t\to\infty$ (i.e., $r_1\to\infty$) by a product of the vibrational eigenfunction of the fragment with an outgoing wave

$$\lim_{r_1\to\infty} \psi_v^-(r_1,r_2,E) = \frac{1}{\hbar}\sqrt{\frac{m_1}{2\pi k_v(E)}}\phi_v(r_2)e^{ik_v(E)r_1}. \tag{9}$$

We may therefore write

$$\sigma_v(E) = \frac{\pi\omega}{3c\epsilon_0}\frac{m_1}{2\pi k_v(E)}\frac{1}{\hbar^2} \times \lim_{t\to\infty} |\langle \phi_v(r_2)e^{ik_v(E)r_1}|\Phi(r_1,r_2,t)\rangle|^2. \tag{10}$$

In Eqs. (9) and (10), $\phi_v(r_2)$ is the vibrational eigenfunction of the fragment. A full derivation of this expression can be found, e.g., in the book by Schinke.[33] We now expand $\Phi(r_1,r_2,t)$ in terms of products of plane waves in the dissociation coordinate r_1 and the vibrational eigenfunctions of the fragment[24]

$$\Phi(r_1,r_2,t) = \sqrt{\frac{1}{2\pi}} \sum_{v'} \int_{k'} A_{v'}(k',t)\phi_{v'}(r_2)e^{ik'r_1}\,dk'. \tag{11}$$

The cross section can then be written as

$$\sigma_v(E) = \frac{m_1}{12\pi c\epsilon_0\hbar^2}\frac{\omega}{k_v(E)} \times \lim_{t\to\infty}\left| \int_{k'}\int_{r_1}\int_{r_2} \phi_v(r_2)e^{-ik_v(E)r_1} \times \sum_{v'} A_{v'}(k',t)\phi_{v'}(r_2)e^{ik'r_1}dr_2dr_1dk'\right|^2. \tag{12}$$

Making use of the exponential definition of the Dirac delta function and the orthonormalization condition of $\phi_v(r_2)$, we arrive at

$$\sigma_v(E) = \frac{m_1}{12\pi c\epsilon_0\hbar^2}\frac{\omega}{k_v(E)} \times \lim_{t\to\infty}\left| \int_{k'} 2\pi\delta(k'-k_v(E))A_v(k',t)dk'\right|^2$$

which leads to

$$\sigma_v(E) = \frac{\pi m_1}{3c\epsilon_0\hbar^2}\frac{\omega}{k_v(E)} \lim_{t\to\infty} |A_v(k_v(E),t)|^2. \tag{13}$$

Equation (13) can easily be generalized to other sets of coordinates by substituting the appropriate reduced mass μ for m_1.

If dissociation can result in n identical fragments, the right-hand side of Eq. (13) should be multiplied by n. The sum of the partial cross sections over v should be equal to the total cross section obtained by Fourier transforming the autocorrelation function [see Eq. (1)], which can be used for testing the accuracy of the calculation.

In the original application of Eqs. (11) and (13) to calculate partial cross sections, the wave packet was propagated on a grid which was large enough to also accommodate the wave packet at asymptotic times. This approach is not practical if recurrences of the wave packet can occur. This problem can be solved[24] by transferring parts of the wave function that reach the asymptotic region to a smaller grid after fixed time intervals by using an appropriate splitting function.[34] In the asymptotic region the wave function is then projected on fragment eigenstates and propagated in momentum space, assuming no interaction between the fragments. Information about recurrences is preserved by continuously adding split off amplitude to the asymptotic wave function, while observing the correct phase relation between the wave functions kept separately on the two grids. An alternative way to calculate v-resolved cross sections can be found in Refs. 27 and 35.

B. Practical implementation and numerical details

The initial vibrational wave function $\Psi_i(r_1,r_2)$ [see Eq. (2)] was generated by a two-dimensional variational procedure using a basis set consisting of product functions of the 15 lowest vibrational eigenfunctions of CH and/or

CD. The one-dimensional vibrational basis functions were obtained by numerical integration, using the CH_2 ground state potential while keeping one bond length fixed at its ground state equilibrium value of 2.03 a_0. This provided 120 symmetrical and 105 asymmetrical functions. The wave function was calculated on a grid and multiplied with the transition dipole moment function $\mu(r_1,r_2)$ to obtain $\Phi(r_1,r_2,t=0)$. Cubic spline interpolation was used to obtain the potential (see Sec. III) and the transition dipole moment function on the 128×128 grid points, which were equally spaced in the range of [1 a_0, 10 a_0]. In order to propagate $\Phi(r_1,r_2,t)$ in time [see Eq. (1)] the method of Tal-Ezer and Kosloff,[36] in which the time-evolving wave packet was expanded in Chebychev polynomials, was used. The fast Fourier transform method[37] was adopted to evaluate the action of the kinetic energy operator on the wave function. For all molecules considered in this work, CH_2, CD_2, and CHD, the total propagation time t is 4000 a.u. of time (1 a.u. $=0.0242$ fs), which corresponds to a spectral resolution ($R=\pi/t$) of 21 meV (170 cm^{-1}). Checks were made to ensure that the calculations were converged with respect to the number of grid points and the total propagation time. The total cross sections calculated directly from the autocorrelation function [see Eq. (1)] had already converged for propagation times of 2000 a.u. However, the total cross section as a sum of partial cross sections [see Eq. (13)] requires the double amount of time of converge.

In order to prevent the wave function from traversing the grid boundaries at larger times, after each time interval of 20 a.u. it was multiplied with the Heather and Metiu cut-off function[34] $f(r_1)f(r_2)$ centered around 8.0 a_0. Similarly, at each subsequent time interval part of the wave function is split off to the asymptotic region ($r_1>8.0$ a_0), using the cut-on function $1-f(r_1)$. The part of the wave packet that is split off is added to the asymptotic wave function $\Psi^a(r_1,r_2,t)$ and, making the assumption that $V=0$ in the asymptotic region, Ψ^a is propagated in momentum space (see also Ref. 24).

To obtain partial cross sections[24] $\Psi^a(r_1,r_2,t)$ is projected on $\phi_v(r_2)$ using

$$\Psi^a(r_1,r_2,t)=\sum_v c_v(r_1,t)\phi_v(r_2) \tag{14}$$

with

$$c_v(r_1,t)=\langle\phi_v(r_2)\,|\,\Psi(r_1,r_2,t)\rangle. \tag{15}$$

The $c_v(r_1,t)$ can be expressed as

$$c_v(r_1,t)=\sqrt{\frac{1}{N}}\sum_k a_v(k,t)e^{ikr_1} \tag{16}$$

in which N is the total number of grid points, both in the interaction region and in the asymptotic region. The coefficients $a_v(k,t)$ can be obtained from the $c_v(r_1,t)$ by a Fourier transform

$$a_v(k,t)=\sqrt{\frac{1}{N}}\sum_n c_v(r_{1n},t)e^{-ikr_{1n}}. \tag{17}$$

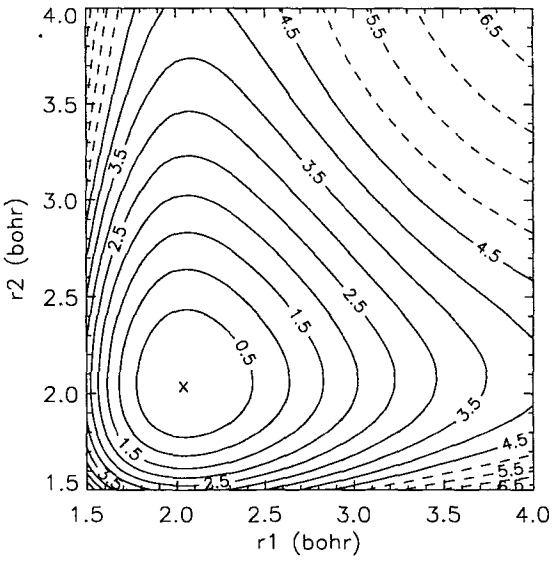

FIG. 1. The calculated potential energy surface for the ground $1\,^3B_1$ state is plotted as a function of both CH bond lengths in a_0, keeping the bond angle fixed at its ground state equilibrium value of 134°. The contour lines are equally spaced with intervals of 0.5 eV. Dashed lines indicate the region which has an energy above the dissociation limit of 4.54 eV, solid lines represent the bound region. The Franck–Condon region is indicated by a cross (×).

The $A_v(k,t)$ coefficients are then related to the $a_v(k,t)$ by[35]

$$A_v(k,t)=\sqrt{\frac{L}{2\pi}}a_v(k,t) \tag{18}$$

in which L is the total length of the grid in momentum space. In writing Eqs. (16)–(18), we have assumed[35] the wave function to be normalized on the grid as

$$\psi_n=\sqrt{\Delta x}\psi(x_n). \tag{19}$$

III. POTENTIAL ENERGY SURFACES

In the dynamics we used potential energy surfaces derived from *ab initio* calculations on a grid including the 11 C–H bond lengths, i.e., 1.25, 1.5, 1.75, 2.03, 2.25, 2.5, 3.0, 3.5, 4.0, 5.0, and 6.0 a_0. The H–C–H bond angle is kept fixed at 134°, the equilibrium value for CH_2. Details of the *ab initio* method and the basis sets employed can be found in Ref. 4. In the region $1.25\ a_0\leqslant r_1,r_2,\leqslant 6\ a_0$, the potential on the grid points used in the dynamics calculation was obtained by cubic spline interpolation of the *ab initio* values. For values of r_1 or r_2 outside this region, the potential was obtained using exponential extrapolation, ensuring the continuity of both the potential and its first derivative.

In Fig. 1, a contour plot of the potential energy surface for the ground state is presented. We find the ground state bound with a limit of 4.57 eV for dissociation into CH and H. No accurate experimental information is available for comparison. Our *ab initio* potential energy surface has its minimum at r_1, $r_2=2.031$ a_0 and $\alpha=135.1°$, in good agreement with experimental values[38] of 2.032 a_0 and 133.9°.

A contour plot of the potential energy surface for the first excited triplet state is shown in Fig. 2 for 1.5

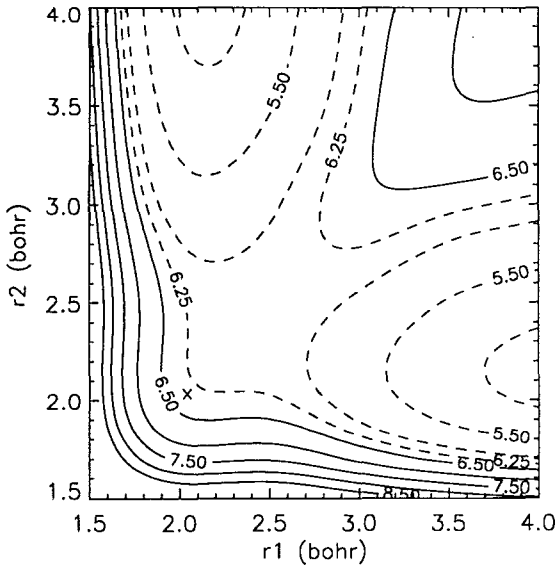

FIG. 2. The calculated potential energy surface for the first excited $1\,^3A_1$ state is plotted as a function of both CH bond lengths in a_0. The bond angle is kept fixed at the ground state equilibrium value of 134°. The contour lines are equally spaced with intervals of 0.5 eV, with one contour line added at 6.25 eV. Dashed lines indicate the region which lies below the Franck–Condon region, solid lines represent the part of the PES that lies above the Franck–Condon region at 6.28 eV. The Franck–Condon region is indicated by a cross (×).

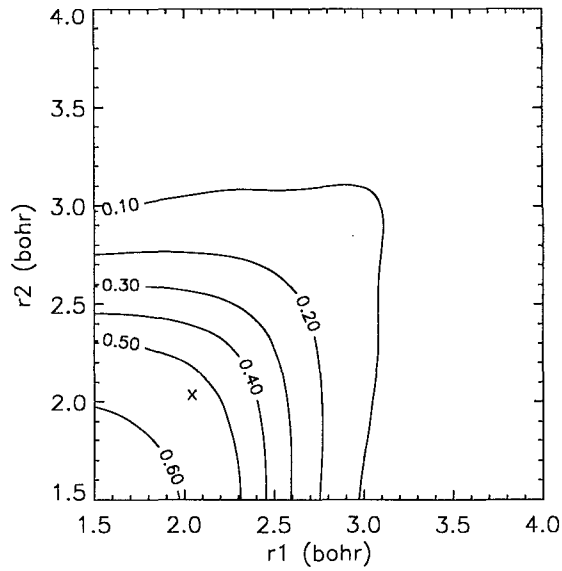

FIG. 3. The calculated transition dipole moment function connecting the ground state with the first excited $1\,^3A_1$ state is plotted as a function of both CH bond lengths in a_0, keeping the bond angle fixed at the equilibrium value of 134°. The contour lines are equally spaced with intervals of 0.1 a.u. (1 a.u.=2.54 D). The Franck–Condon region is indicated by a cross (×).

$a_0 < r_1, r_2 < 4\,a_0$. The vertical excitation energy is 6.33 eV. It is evident that the two exit channels are dissociative toward the ground state of CH+H without a barrier. In the Franck–Condon region, the potential energy surface is rather flat. At $\alpha = 134°$, the saddle point lies at r_1, $r_2 = 2.35\,a_0$, and the energy at the saddle point E_{sa} is 6.18 eV. The symmetric stretch vibration is bound, with dissociation into separate atoms possible only at 8.2 eV.

In Fig. 3, a contour plot of the transition dipole moment function connecting the ground state with the $1\,^3A_1$ state is presented. In the Franck–Condon region, the transition dipole moment is large; in a one-configuration description the $\tilde{X}\,^3B_1 \rightarrow 1\,^3A_1$ transition at the equilibrium geometry corresponds to a single orbital excitation, $1b_1 \rightarrow 4a_1$. Since $1b_1$ is mainly carbon $2p$ and $4a_1$ mainly carbon $3s$, the transition moment is nearly equal to the large atomic carbon value. If one or both CH bonds are stretched, the transition moment decreases rapidly because the transition becomes forbidden. The variation of the transition moment with the C–H bond length is stronger than for photodissociation of water in the first absorption band (compare Fig. 5 of Ref. 7 with our Fig. 3). Therefore, inclusion of the dependence of the transition dipole moment on r should be more important than in the case of water.

IV. RESULTS AND DISCUSSION

A. Vibrationless CH_2

The autocorrelation function for photodissociation of vibrationless CH_2 is shown in Fig. 4, and the total photodissociation cross section calculated using the two-dimensional wave packet method in Fig. 5. As can be seen from Fig. 4, the dissociation through the $1\,^3A_1$ state occurs very rapidly: after 15 fs less than 1% of the wave packet is still in the Franck–Condon region. Due to a recurrence of

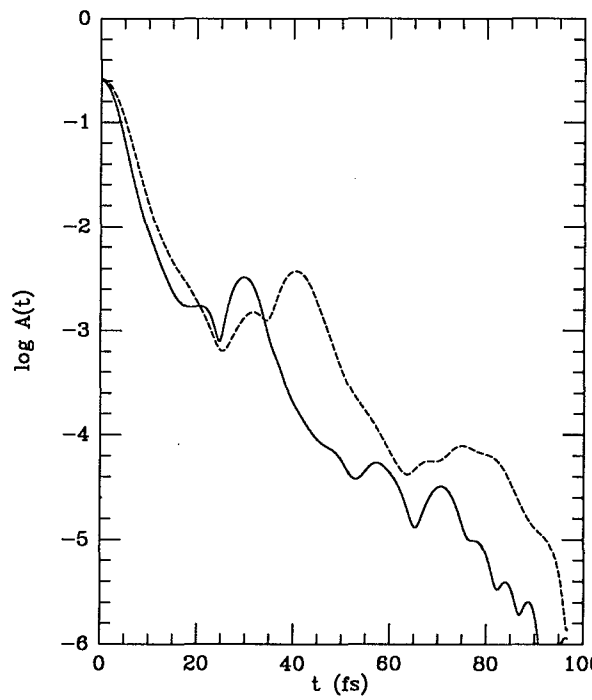

FIG. 4. The logarithm (base 10) of the absolute value of the autocorrelation function $A(t) = |\langle \Phi(r_1, r_2, t=0) | \Phi(r_1, r_2, t) \rangle|$ is plotted as a function of time in fs. $A(t)$ is in atomic units. The solid line is for photodissociation of CH_2, the dashed line for photodissociation of CD_2. The initial value of the autocorrelation functions is the expectation value of the square of the transition dipole moment function.

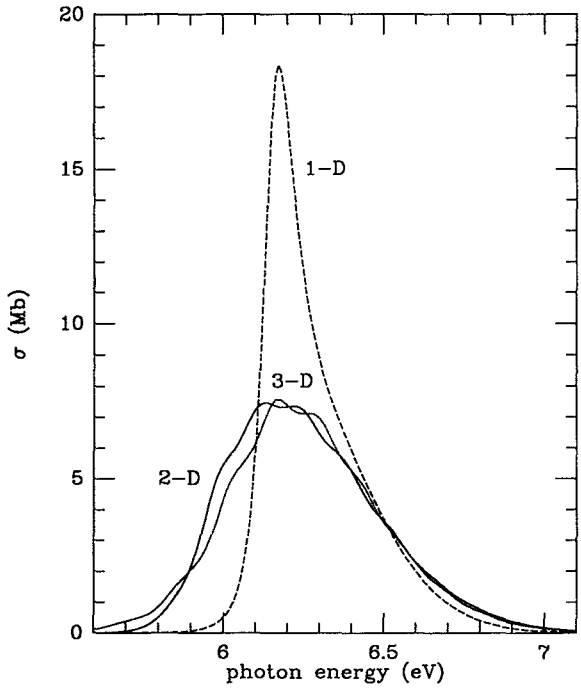

FIG. 5. Total cross sections (in Mb, 1 Mb$=10^{-18}$ cm^2) for photodissociation of vibrationless CH_2 are plotted as a function of the energy $\hbar\omega$ of the exciting radiation in eV. The solid line represents the results of the two-dimensional wave packet calculations, the dashed line the results obtained from one-dimensional dynamics calculations, and the dotted line represents results obtained from three-dimensional wave packet calculations.

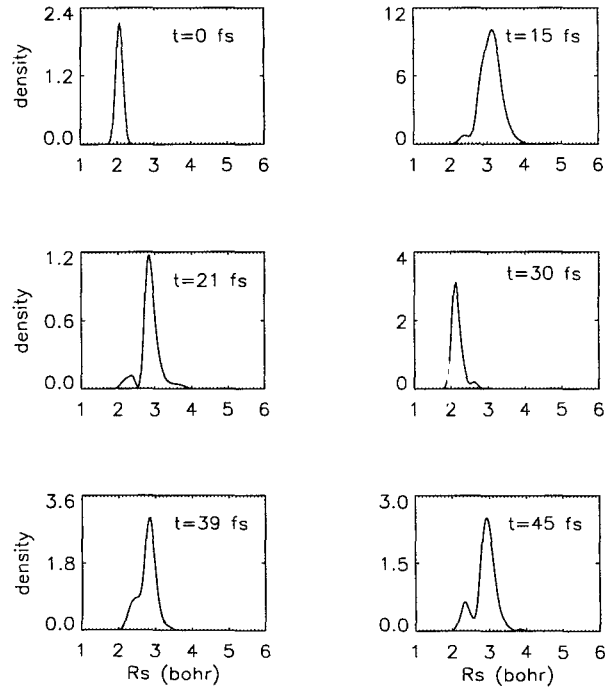

FIG. 6. The density of the wave function $|\Phi(r_1,r_2)|^2$ along the line $r_1=r_2$ is plotted as a function of the symmetric stretch coordinate $R_s=(r_1+r_2)/2$ for $t=0$, 15, 21, 30, 39, and 45 fs. To obtain figures on a reasonable scale, the density was multiplied with 10^3, 10^3, 10^4, 10^5, and 10^6 for $t=15$, 21, 30, 39, and 45 fs, respectively. The results are for vibrationless CH_2.

the wave packet into the Franck–Condon region, the autocorrelation function shows a maximum at $t\approx 29$ fs. This time interval corresponds to periodic motion with a frequency of 1150 cm^{-1}, in agreement with the observed energy spacing (0.14 eV$=$1130 cm^{-1}) of the peaklike features observed in the two-dimensional absorption spectrum.

The structure seen in the two-dimensional absorption spectrum was also found in our three-dimensional wave packet calculations.[5] One-dimensional model calculations which considered the symmetric stretch vibration along the cut ($r_1=r_2$, $\alpha=134°$) showed that the structure seen in Fig. 5 can be explained by the symmetric stretch vibration being bound on the excited state $1\,^3A_1$ surface. The energy spacing between the excited state vibrational levels calculated with the model was 1100 cm^{-1}, and the height of the peaklike features in the three-dimensional spectrum was in qualitative agreement with the Franck–Condon factors $|\langle v_s''=0|\mu|v_s'\rangle|^2$ calculated using the model (v_s is the quantum number for the symmetric stretch vibration). This model has been used before in calculations on photodissociation of water,[39] and is explained in more detail in Sec. IV B.

In Fig. 6, we present further evidence that the recurrence seen in Fig. 4 is indeed due to the symmetric stretch vibration. As can be seen from this figure, at $t\approx 15$ fs along the line $r_1=r_2$ most of the wave packet has moved away from the Franck–Condon region (near $r_1=r_2=2.03\ a_0$), while at $t\approx 30$ fs most of the wave packet along $r_1=r_2$ has returned to the Franck–Condon region. Thus, the peaklike features seen in both the two-dimensional absorption spectrum and the three-dimensional spectrum[5] represent transitions to metastable states on the excited state surfaces which differ in the degree of excitation of the symmetric stretch vibration. The same has also been found for water in the first absorption band.[8] These results represent yet another confirmation of Pack's explanation[40] of the diffuse structure observed in photodissociation spectra of polyatomic molecules. The diffuse "peaks" in the spectra represent transitions in which vibrations which are bound on the excited state surface are excited.

In Fig. 5, the total two-dimensional cross section calculated using Eq. (1) is compared with results from both a three-dimensional[5] and a one-dimensional dynamics calculation. The two-dimensional results are greatly similar in shape to the three-dimensional results, apart from a shift of 0.05 eV in the position of the maxima, which is due to the difference in the vibrational energy available in the bending mode for the ground and excited states. In the one-dimensional calculation, one C–H bond length was kept fixed at the equilibrium bond length of CH_2, 2.03 a_0, while fixing the bond angle at 134°. As a result, the one-dimensional spectrum lacks the diffuse structure seen in the two-dimensional and three-dimensional spectra. As can be seen from Fig. 5, the one-dimensional calculation also fails to reproduce the overall shape of the spectrum. Although the integrated cross sections are more or less the

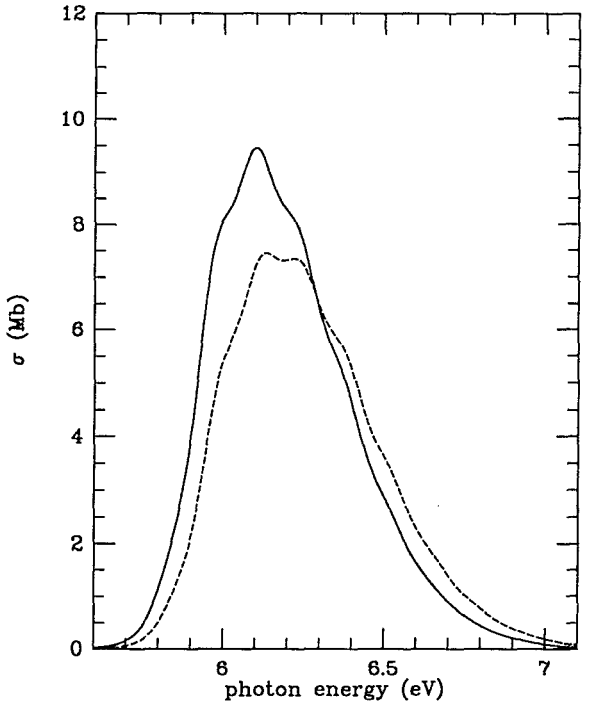

FIG. 7. The total cross section (in Mb, 1 Mb$=10^{-18}$ cm^2) for photodissociation of vibrationless CH_2 is plotted as a function of the energy $\hbar\omega$ of the exciting radiation for two different calculations. The dashed line represents results of calculations using the full coordinate dependence of $\mu(r_1,r_2)$. The solid line represents results of calculations using $\mu(r_1,r_2)=\mu_e$.

same and the peak maxima are at approximately the same excitation energy, the one-dimensional spectrum has a peak which is much higher but also more narrow, mostly because the one-dimensional spectrum starts at higher excitation energies. The reason that the two-dimensional spectrum starts at lower excitation energies is that the initial two-dimensional wave packet also samples the excited state surface at configurations where the potential is lower by allowing both bond lengths to stretch simultaneously (see Fig. 2).

In Fig. 7, total cross sections for photodissociation calculated with the full transition dipole moment function surface $\mu(r_1,r_2)$ are compared with cross sections obtained using $\mu_e(r_1=r_2=r_e)$ with $r_e=2.03\ a_0$ (the experimental equilibrium bond length). As can be seen from this figure, neglecting the coordinate dependence of $\mu(r_1,r_2)$ leads to systematic errors in the total cross section: the spectrum calculated using $\mu=\mu_e$ is higher at low excitation energies and lower at excitation energies larger than 6.35 eV. The reason for this trend can be found in the coordinate dependence of $\mu(r_1,r_2)$, $\mu(r_1,r_2)$ being larger than μ_e for $r_1,r_2<r_e$ and smaller than μ_e for $r_1,r_2>r_e$. The integrated cross section calculated using $\mu=\mu_e$ is larger by about 10%.

In conclusion, we find that one-dimensional dynamics calculations are insufficient for obtaining the absorption spectrum, since they even fail to reproduce the overall shape of the spectrum. In two-dimensional wave packet calculations, neglecting the coordinate dependence of μ leads to systematic errors. But, as previous calculations showed,[5] including the coordinate dependence of μ with the second degree of freedom (allowing both r_1 and r_2 to change while keeping α fixed at α_e) while employing the LHL approximation yields total cross sections which are accurate to within 2% compared to three-dimensional ($J=0$) wave packet results. Similarly good agreement between two-dimensional and three-dimensional spectra was found before in calculations on photodissociation of water.[14]

The two-dimensional absorption spectrum shows a maximum at 6.13 eV and a secondary maximum at 6.22 eV (see Fig. 5). These energies almost coincide with the excitation energies associated with two unidentified peaks occurring in the 3+1 resonance enhanced multiphoton ionization (REMPI) spectrum of CH_2 measured by Irikura and Hudgens,[23] provided that these peaks represent two-photon transitions rather than three-photon transitions. The two observed peaks occur at wavelengths of 396.5 and 403.5 nm, corresponding to excitation energies of 6.25 and 6.15 eV, respectively. While it could not be completely ruled out that the peak at 6.15 eV is due to photodissociation of CH_3 which is also present in the experiment, the other peak was assigned to CH_2, though not yet to any particular transition. We cannot compare our calculated spectra directly with the REMPI spectrum since the latter should also reflect the Franck–Condon transition probabilities to CH_2^+ states. Nevertheless, it should be noted that the unidentified peaks in the REMPI spectrum[23] possibly represent the first experimental observation of absorption of CH_2 through the $1\,^3A_1$ state. Hopefully, the 2+1 REMPI experiments[41] on CH_2 can be extended to larger wavelengths, and confirm our tentative assignment and the prediction already made by Römelt *et al.*,[3] that photodissociation of CH_2 through the $1\,^3A_1$ state is an efficient process occurring at excitation energies close to 6.38 eV.

Partial cross sections which are resolved with respect to the vibrational state of the fragment are presented in Fig. 8. As can be seen from this figure, the final vibrational state distribution becomes hotter at larger excitation energies, the $v=1/v=0$ ratio becoming larger than unity at excitation energies above 6.46 eV. At larger excitation energies, dissociation will proceed from initial geometries with both r_1 and r_2 small and close to the line $r_1=r_2$ (the saddle point in the excited state surface lies at $r_1=r_2=2.35\ a_0$), leading to excitation of both bonds. The smaller r_1 and r_2 are initially, the stronger the coupling between the dissociating mode and the mode that remains bound will be, and the more the diatomic fragment will be excited vibrationally.[7] The larger final state interaction at higher excitation energies also explains why the structure seen in the v resolved cross sections is more pronounced at the red end of the spectrum.[9] At an excitation energy close to a peak in the total absorption spectrum, a metastable state characterized by the quantum number v_s' is excited. Through the overlap with fragment vibrational wave functions, there will usually be a Franck–Condon-like preference for producing CH in particular v states. The weaker the final state interaction, the more this preference will be conserved during the dissociation process, which should result in a

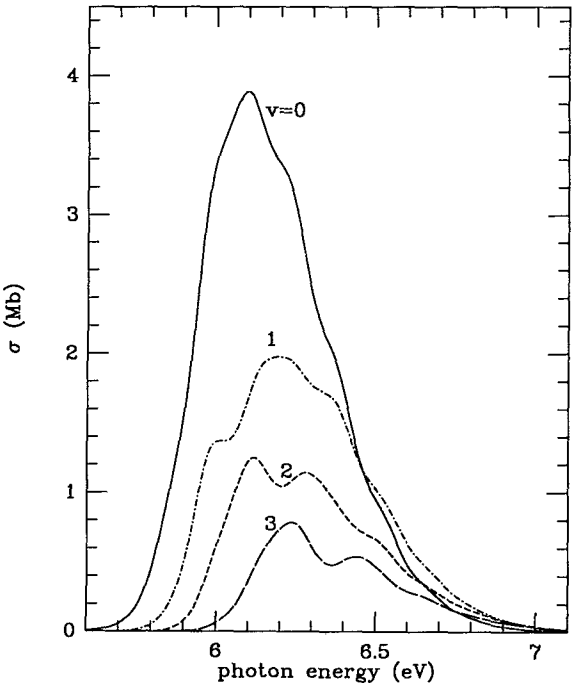

FIG. 8. Partial cross sections (in Mb, 1 Mb$=10^{-18}$ cm^2) for photodissociation of vibrationless CH_2 are plotted as a function of $\hbar\omega$ in eV, for v=0–3.

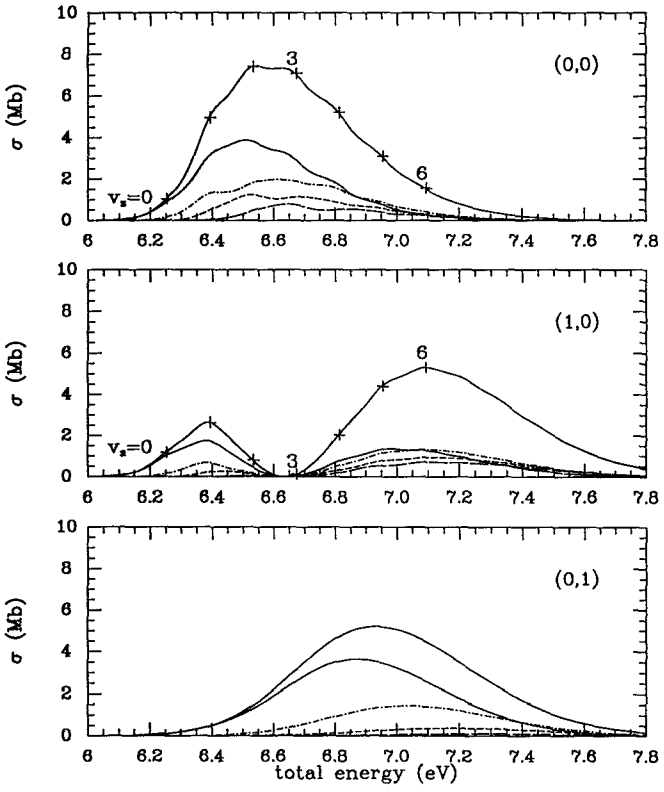

FIG. 9. Total cross sections (in Mb, 1 Mb$=10^{-18}$ cm^2) for photodissociation of CH_2 with $(v_s'', v_a'')=(0,0)$, (1,0), and (0,1) are presented as functions of the total energy E of the molecule. The positions of the diffuse spectral features are marked by + symbols. For conversion of E to $\hbar\omega$, see Sec. IV B. Partial cross sections are also given, for v=0 (solid line), v=1 (dot–dashed line), v=2 (dashed line), and v=3 (long-dashed line).

strong peaklike feature in at least one of the v resolved cross sections at the same excitation energy. The larger the excitation energy, the stronger the final state interaction, and the more blurred the peaklike features in the partial cross sections will become.

B. Vibrationally excited CH_2

Total cross sections for photodissociation starting from the $(v_s'', v_a'')=(1,0)$ and (0,1) states are compared with cross sections for dissociation of the vibrational ground state in Fig. 9. To facilitate comparison and because the time-independent wave function in the excited state is determined by the total energy $E=E_i+h\nu$, the cross sections are plotted as functions of the total energy of the molecule. The energy of the exciting radiation can be obtained for each case by considering the initial vibrational energy of the molecule, E_i, which is 0.41 eV for the ground state, 0.80 eV for the (1,0) and (0,1) states. Note that E_i is the initial vibrational energy of the molecule, since the zero of the potential energy surfaces is taken as the value of the ground state potential at its equilibrium geometry.

As can be seen from Fig. 9, $\sigma(E)$ behaves quite differently as a function of E for dissociation of the (1,0) state compared with the (0,0) state. This difference can be understood from a two-dimensional version of the Franck–Condon principle as formulated by Pack,[39,40] and from the multidimensional reflection approximation as formulated by Heller.[26,42]

Since the symmetric stretch motion remains bound on the excited state surface, the total cross section for photodissociation can be expressed as[40]

$$\sigma(E) \sim \sum_{v_s'} |\langle \psi_{v_s'}(E) | \mu | \Psi_i \rangle|^2, \tag{20}$$

where $\psi_{v_s'(E)}$ is the wave function for nuclear motion in the excited electronic state labeled by the symmetric stretch quantum number v_s', and E is its total energy. If the assumption is made that the dissociation proceeds vibrationally adiabatic and that near the Franck–Condon region μ only depends on the symmetric stretch coordinate R_s, Eq. (20) may be written as[40]

$$\sigma(E) \sim \sum_{v_s'} |\langle \chi(z,E_{zf}) | v_a''(z) \rangle \langle v_s'(x) | \mu(x) | v_s''(x) \rangle|^2. \tag{21}$$

In Eq. (21), x and z are so-called natural reaction coordinates.[43] At the saddle point x is parallel to R_s and z is parallel to the antisymmetric stretch coordinate R_a. Further, $v_s'(x)$ and $v_s''(x)$ represent symmetric stretch vibrational wave functions in the excited state and ground state, respectively, $v_a''(z)$ is the antisymmetric stretch vibrational

TABLE I. Franck–Condon factors $\langle v_s'|\mu|v_s''\rangle^2$ are given for the overlap of the upper state v_s' states with the lower $v_s''=0$ and $v_s''=1$ states. The Franck–Condon factors were normalized to a sum (over v_s') of one, and result from one-dimensional model calculations (Ref. 5) for the symmetric stretch coordinate. An approximate assignment of the position E_{sp} of the peaklike features associated with transitions to v_s' states is also given.

v_s'	$\langle v_s'\|\mu\|v_s''=0\rangle^2$	$\langle v_s'\|\mu\|v_s''=1\rangle^2$	E_{sp} (eV)
0	0.18	0.21	6.25
1	0.30	0.10	6.39
2	0.25	0.00	6.53
3	0.15	0.08	6.67
4	0.07	0.17	6.81
5	0.03	0.17	6.95
6	0.01	0.13	7.09

function of the electronic ground state, and $\chi(z,E_{zf})$ is a continuum wave function of the dissociation coordinate with an amount of energy E_{zf} available for the unbound motion in the z direction. Now consider the size of the overlap $\langle\chi(z,E_{zf})|v_a''(z)\rangle$. The potential for unbound motion can be taken as a symmetric barrier function in z which is zero in the dissociation limit and equal to E_b at the top of the barrier. It can be shown that, for $v_a=0$, $\langle\chi(z,E_{zf})|v_a''(z)\rangle$ is large only at energies E_{zf} close to E_b (see Figs. 4 and 5 of Ref. 40). Typically, $|\langle\chi(z,E_{zf})|v_a''(z)\rangle|^2$ is a slightly asymmetric function of E_{zf} which is skewed towards higher energies with a full width at half-maximum equal to $1/\tau$, where τ is the lifetime of the metastable state characterized by the quantum number v_s' (see Fig. 5 of Ref. 40). The overall shape of the spectrum then results from overlapping, asymmetric peaks, the height of which is determined by the size of the Franck–Condon factors $|\langle v_s'(x)|\mu(x)|v_s''(x)\rangle|^2$. These factors can be calculated using a one-dimensional model Hamiltonian which considers the symmetric stretch motion at $r_1=r_2$ and $\alpha=\alpha_e$.[39] Franck–Condon factors which were calculated in this way (for details see Ref. 5) are tabulated in Table I. As can be seen from this table, for $v_s''=0$ the Franck–Condon factors first increase with v_s' and then decrease again, which explains the overall shape of the (0,0) and (0,1) spectra in Fig. 9. On the other hand, due to the node in the vibrational wave function in the coordinate which remains bound on the excited state surface, for $v_s''=1$ the Franck–Condon factors first increase and decrease, and then increase again with v_s', resulting in the bimodal shape of the (1,0) spectrum. Note that the minimum of the (1,0) spectrum coincides with the maximum of the (0,0) spectrum, which is exactly what is expected from the Franck–Condon model.

It should be noted that the two-dimensional Franck–Condon model is fundamentally different from the one-dimensional reflection principle, in that in the Franck–Condon model the overall shape of the spectra is determined by the size of bound–bound overlap functions rather than by bound–continuum overlap functions. On the other hand, the multidimensional reflection principle as formulated by Heller[26,42] also yields correct predictions concerning the overall shape of the spectrum. According to this model, a node in the ground state vibrational wave function leads to a low-resolution bump in the spectrum if it is located perpendicular to the "downhill direction" on the upper surface. Starting from the Franck–Condon region, the initial downhill direction is along the symmetric stretch, the antisymmetric stretch becoming dissociative closer to the saddle point. For a thorough discussion of how the nodal structure of the electronic ground state vibrational wave function determines the overall shape of the spectrum, see Chap. 13 of Ref. 33.

The (0,0) and (1,0) spectra show considerable structure with peaklike features which should be located approximately at

$$E_{\rm sp}=E_{\rm sa}+E_v(v_s'), \tag{22}$$

where $E_{\rm sa}$ is the potential energy of the excited state at the saddle point (6.18 eV) and $E_v(v_s')$ is the symmetric stretch vibrational energy. The features in the spectra were found to be located at $6.18+(v_s'+1/2)\times 0.14$ eV, in agreement with Eq. (22) and the energy spacing of 0.14 eV calculated in Ref. 5. Thus, the two-dimensional Franck–Condon model yields predictions that are in qualitative agreement with the calculated absorption spectra: the calculated Franck–Condon factors correctly predict the overall shape of the spectra, which show features at excitation energies correctly predicted by one-dimensional model calculations using a symmetric stretch Hamiltonian.

It is also possible to make the further approximation that the overlap of the peaks due to transitions to states with different v_s' is small. This will be the case if the lifetime of the metastable states is large. If this approximation would apply, the height of the absorption spectrum at the position of the features $E_{\rm sp}(v_s')$ should be in quantitative agreement with the value of the Franck–Condon factors $|\langle v_s''|\mu|v_s'\rangle|^2$. But, as can be seen from comparing Table I and Fig. 9, the Franck–Condon factors do not correctly predict the size of the absorption spectra. Although the Franck–Condon factors predict that for dissociation of the (0,0) state $\sigma(E)$ should be largest at $E_{\rm sp}(v_s'=1)$ and $E_{\rm sp}(v_s'=2)$, $\sigma(E)$ is much larger at $E^{\rm sp}(v_s'=3)$ than at $E_{\rm sp}(v_s'=1)$. Similarly, for dissociation of the (1,0) state, $\sigma(E)$ is much larger at $E_{\rm sp}(v_s'=6)$ than at $E_{\rm sp}(v_s'=4)$, in contrast with the prediction of the Franck–Condon model. Clearly, the overlap of the different v_s' peaks should also be taken into account. The width of the peaks can be calculated from the lifetime of the metastable states. This lifetime τ can be estimated from the decay of the autocorrelation function from $t=0$ to $t=29$ as $\tau=275$ a.u. of time, yielding a width $\Gamma=\pi\hbar/\tau$ of approximately 0.3 eV. This width is larger than the energy spacing of the features which explains why the structure is so poorly resolved. Also, the asymmetry of the peaks already mentioned explains why the peaks with larger v_s' tend to be higher than predicted (the peaks are skewed towards larger energies). Our CH_2 results are similar to those obtained previously for (0,0) water.[39] Likewise, for H_2O the Franck–Condon

factors $|\langle v_s''|\mu|v_s'\rangle|^2$ did not yield quantitatively correct predictions of the size of σ at the energies where the features are located. On the other hand, the spectrum calculated using Eq. (21) (i.e., taking the overlap between the peaks also into account) was in good agreement[39] with the results of two-dimensional dynamics calculations.[7]

In contrast to the (0,0) and (1,0) spectra, the (0,1) spectrum shows no structure. The reason for this is that the initial wave packet has a node along the line $r_1=r_2$ and is located in the exit channels. Dissociation will then proceed without part of the wave function recurring into the Franck–Condon region after vibrating along the R_s coordinate, and the resulting autocorrelation function decreases monotonically with t. For structure to be present in the spectrum, it is necessary that a part of the wave function recurs into the Franck–Condon region at least once.

Cross sections that are resolved with respect to the vibrational state of the fragment are also presented in Fig. 9 for $v(CH)=0$–3. The observed trends are similar to those found previously for photodissociation of water.[7] Although dissociation of the (0,1) state proceeds from an initially vibrationally excited molecule, the resulting CH fragment is vibrationally much colder than the CH fragment resulting from photodissociation of (0,0) CH_2. This is because in dissociation of (0,1) CH_2, the initial wave packet is already located in the exit channel, where the coupling between the dissociating coordinate mode and the fragment mode is weak. Note that the CH fragment resulting from photodissociation of (1,0) CH_2 is vibrationally quite hot at larger energies: the $v=1/v=0$ ratio becomes larger than unity at $E>7.1$ eV. Also note that at similar energies the CH fragments produced in dissociation of (0,0) CH_2 are just as hot or even hotter, the $v=1/v=0$ ratio becoming larger than unity at $E>6.9$ eV.

C. Vibrationless CD_2

In Fig. 4, the autocorrelation function for photodissociation of vibrationless CD_2 is compared with that of CH_2, and in Fig. 10 the total cross sections for photodissociation of vibrationless CD_2 and CH_2 are compared. Because the frequency of the symmetric stretch vibration on the excited state potential energy surface of CD_2 is lower than that of CH_2, the recurrence of the wave packet into the Franck–Condon region takes place after a larger time interval for CD_2 (40 fs, see Fig. 4). The recurrence time corresponds to periodic motion of frequency 830 cm^{-1} (0.10 eV), in agreement with the energy spacing between the peaklike features seen in the absorption spectrum (0.09 eV, see Fig. 10). The larger reduced mass of CD_2 causes the CD_2 spectrum to be narrower than the CH_2 spectrum. The range of excited state potential energies sampled by the initial CD_2 wave packet is narrower because it is confined to a region of coordinate space more narrow in r_1 and r_2. Because the dependence of the transition dipole moment function on the coordinates is not too strong, the oscillator strengths are approximately the same for CD_2 and CH_2. Therefore, the CD_2 spectrum is not only narrower but also higher, showing a maximum of $\sigma=9.9$ Mb (1 Mb$=10^{-18}$ cm^2) at

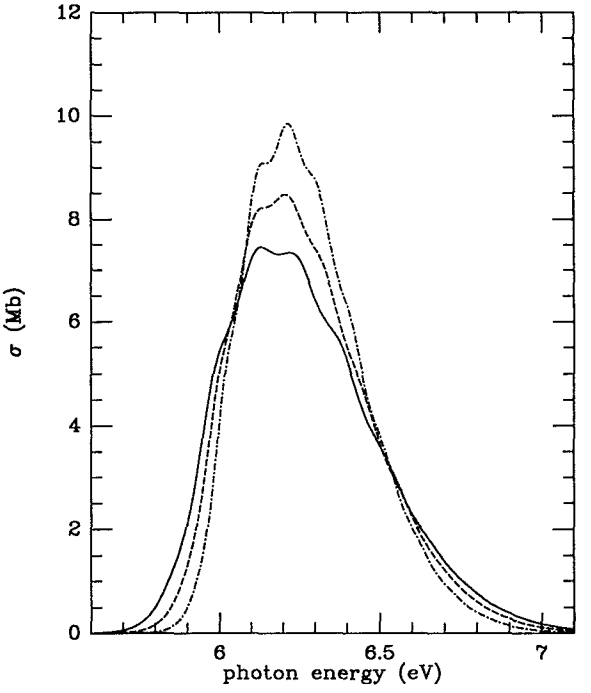

FIG. 10. Total cross sections (in Mb, 1 Mb$=10^{-18}$ cm^2) are compared for photodissociation of vibrationless CH_2 (solid line), CD_2 (dot–dashed line), and CHD (dashed line). The cross sections are plotted as a function of the energy of the exciting radiation $\hbar\omega$ in eV.

an excitation energy of 6.21 eV, whereas CH_2 has a maximum of $\sigma=7.4$ Mb at an excitation energy of 6.13 eV. Note also that the structure near the maximum in the spectrum is reversed for CD_2. The CD_2 spectrum has a maximum at $\hbar\omega=6.21$ eV, and a secondary maximum at $\hbar\omega=6.14$ eV, while for CH_2 these values are 6.13 and 6.22 eV, respectively.

As was the case for CH_2, in a 2+1 REMPI spectrum of CD_2 photodissociation through the first excited triplet state should result in a peak at laser wavelengths close to 400 nm. In the CD_2 REMPI spectrum presented by Irikura and Hudgens,[23] a peak is present at $\lambda\approx401$ nm which is not assigned to any transition. Once again, it is our hope that future measurements will clarify whether this peak is due to the $1\,^3A_1\leftarrow\tilde{X}\,^3B_1$ transition of CD_2.

Vibrationally resolved cross sections for photodissociation of CD_2 are presented in Fig. 11. For CD_2, at similar excitation energies the vibrational distribution is shifted toward higher v than for CH_2 (see also Fig. 8). The reason for this is simply that the frequency of the CD fragment is lower. Depositing a similar amount of vibrational energy requires on average excitation to a higher v state for CD_2. Similar results were also obtained for H_2O and D_2O.[7]

The vibrational distribution of the fragments formed is non-Boltzmann. Therefore, to determine which fragment, CD or CH, is hotter, the average vibrational energies $\bar{E}_v$ of the fragments are compared for CH_2 and CD_2 as functions of the total energy E (see Fig. 12). The average vibrational energy is derived from the partial cross sections $\sigma_v(E)$ and the fragment vibrational energies ϵ_v according to

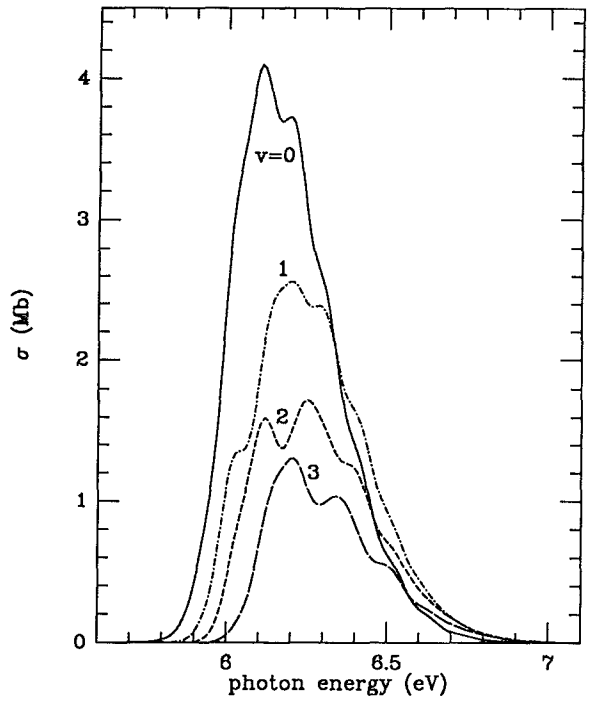

FIG. 11. Partial cross sections (in Mb, 1 Mb$=10^{-18}$ cm^2) for photodissociation of vibrationless CD_2 are plotted as a function of $\hbar\omega$ in eV, for $v=0$–3.

$$\bar{E}_v(E)=\sum_v \epsilon_v \sigma_v(E)/\sigma(E). \tag{23}$$

For the fragments resulting from the dissociation of both CH_2 (solid line) and CD_2 (long-dashed line), the average vibrational energies have a linear dependence on the total energy in the range 6.2–7.1 eV. At total energies below the saddle point energy $E_s=6.18$ eV, the average vibrational energies correspond to the zero point vibrational energies of the fragments. For total energies above E_s, the differences in the slopes show that the energy of the exciting radiation is converted more effectively into vibrational energy for CD_2 than for CH_2. The higher average vibrational energy of CD arises from a larger interaction time.[16] Because D is heavier, the coupling between the dissociating mode and the fragment mode, which causes the vibrational excitation in CD, acts for a longer period of time, resulting in increased excitation.

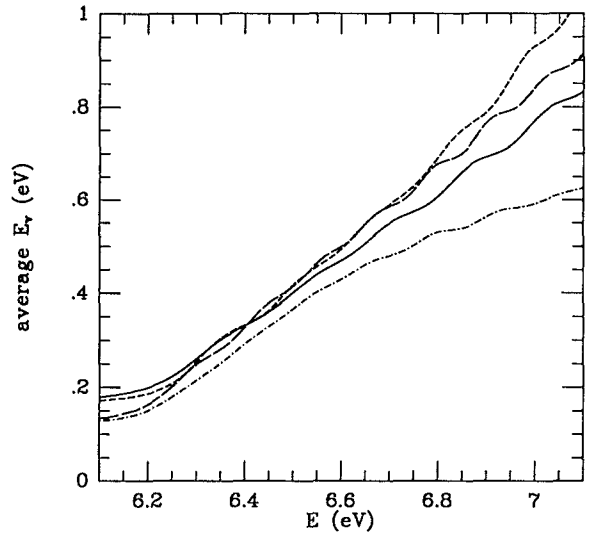

FIG. 12. Average vibrational energies are plotted as functions of the total energy E [see Eq. (23)] for CH fragments resulting from photodissociation of CH_2 (solid line) and CHD (dashed line) and for CD fragments resulting from dissociation of CD_2 (long-dashed line) and CHD (dot–dashed line).

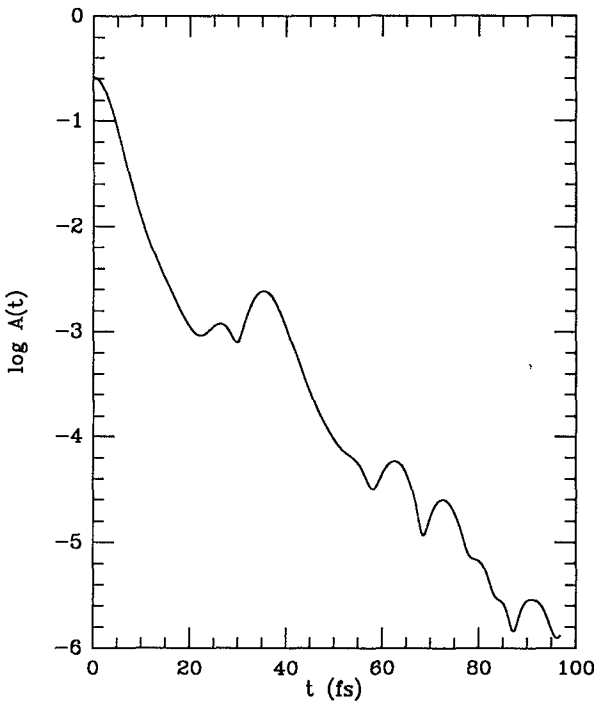

FIG. 13. The logarithm (base 10) of the absolute value of the autocorrelation function $A(t)=|\langle\Phi(r_1,r_2,t=0)|\Phi(r_1,r_2,t)\rangle|$ is plotted as a function of the propagation time t in fs for photodissociation of CHD. $A(t)$ is in atomic units. The initial value of the autocorrelation function is the expectation value of the square of the transition dipole moment function.

D. Vibrationless CHD

The autocorrelation function for dissociation of CHD is displayed in Fig. 13, and the absorption spectrum of CHD is compared to that of CH_2 and CD_2 in Fig. 10. As can be seen from Fig. 10, the spectrum is halfway in between that of CD_2 and CH_2 in both narrowness and height, as would be expected. The total cross section for photodissociation of CHD has a maximum of 8.5 Mb at $\hbar\omega=6.21$ eV and a shoulder of 8.2 Mb at $\hbar\omega=6.14$ eV. The autocorrelation function shows a clear maximum at $t=35$ fs and a second maximum at $t=62$ fs, corresponding to periodic motion of frequency 0.12 and 0.07 eV, respectively.

Cross sections σ_{CD} and σ_{CH} for producing CD and CH are plotted in Fig. 14, and the branching ratio CD/CH is plotted in Fig. 15. To obtain the cross sections, the partial cross sections σ_v [see Eq. (13)] were summed for both

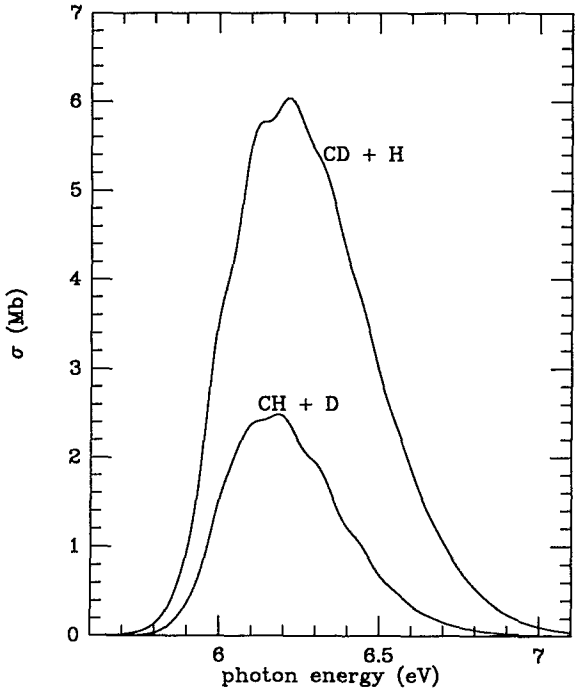

FIG. 14. Cross sections (in Mb, 1 Mb$=10^{-18}$ cm^2) σ_{CH} and σ_{CD} are compared for dissociation of vibrationless CHD into CH+D and into CD+H, respectively. The cross sections are plotted as a function of the energy of the exciting radiation $\hbar\omega$ in eV.

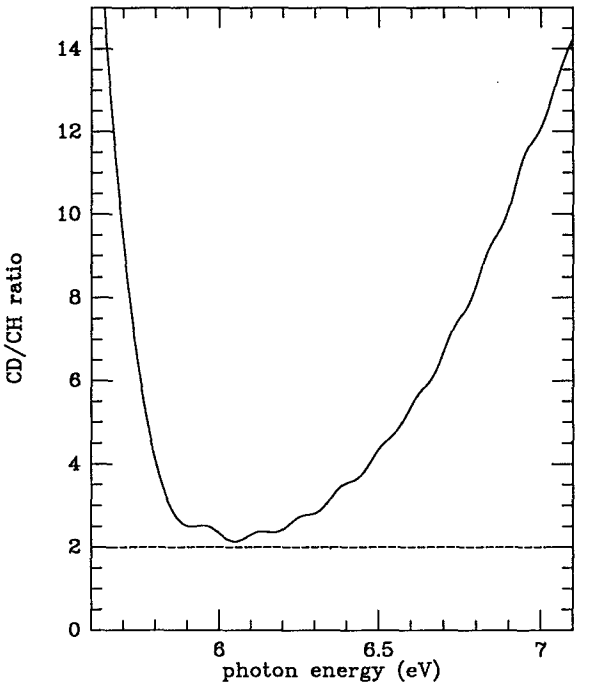

FIG. 15. The CD/CH branching ratio is plotted as a function of the energy of the exciting radiation $\hbar\omega$ in eV for photodissociation of vibrationless CHD.

fragments. The sum of the cross sections σ_{CD} and σ_{CH} differs less than 0.1 Mb from the value for the total photodissociation cross section obtained from the autocorrelation function [see Eq. (1)], which is shown in Fig. 10. In agreement with results previously obtained for photodissociation of water,[16,17] there is a clear preference for the production of CD over the entire range of the spectrum. The branching ratio CD/CH is large at both low and high excitation energies, and reaches a lower limit of two at $\hbar\omega \approx 6.05$ eV. At small (large) excitation energies, according to the reflection principle both r_1 and r_2 are large (small) and approximately equal, so that the forces which push D and H away from the Franck–Condon region are approximately the same. But because its mass is lower by a factor of 2, the acceleration of the H atom is approximately twice as large, which explains the enhanced branching ratio at small and at large excitation energies.[17] It is not entirely clear why the branching ratio should reach a lower limit of exactly two as was also found for HOD.[16,17] It is tempting to speculate[16] that this lower limit somehow results from the ratio of the accelerations of H and D for $r_{OH}=r_{OD}$, which is also two,[16] but it is not clear why this should be so.

The cross sections σ_{CD} and σ_{CH} (see Fig. 14) both show diffuse structure. The energy spacings are approximately 0.09 eV in σ_{CD} and 0.11 eV in σ_{CH}, in qualitative agreement with the frequencies calculated from the maxima in the autocorrelation function (Fig. 13) located at $t=62$ and 35 fs. The frequency of 0.11 eV should approximately equal the CH vibrational frequency of CHD in the excited electronic state while located in the Franck–Condon region, while the CD vibrational frequency of the dissociating CHD molecule should be approximately 0.08 eV.[17,40]

Partial cross sections σ_v are shown in Fig. 16 for the CD fragment and in Fig. 17 for the CH fragment. As can be seen from comparing Figs. 16 and 11, the vibrational level distribution of the CD fragment produced by dissociation of CD_2 is somewhat hotter than that of CHD. This is seen even more clearly in Fig. 12 where the average vibrational energies of the CH and the CD fragments resulting from photodissociation of CH_2, CD_2, and CHD are compared as functions of the total energy. The curve for CD resulting from photodissociation of CHD (dot-dashed line) has at lower total energies the same slope as that of CH produced by dissociation of CH_2. This is in agreement with the model discussed in the last paragraph of Sec. IV C: the amount of energy disposed in vibration of the fragment is determined by the interaction time, which is short in both cases. However, at higher energies the dependence of the average vibrational distribution for CD from CHD on the total energy is no longer linear; the energy disposed in the exciting radiation is no longer as effectively converted to CD vibrational energy as at lower energies. This is also in accord with the model where the amount of vibrational excitation of the fragment is determined by the interaction time: the larger the total energy, the longer the interaction time will be for all the isotopomers of CH_2, and consequently the larger the difference in the interaction time between any two isotopomers will be. A large excitation energy results in a long interac-

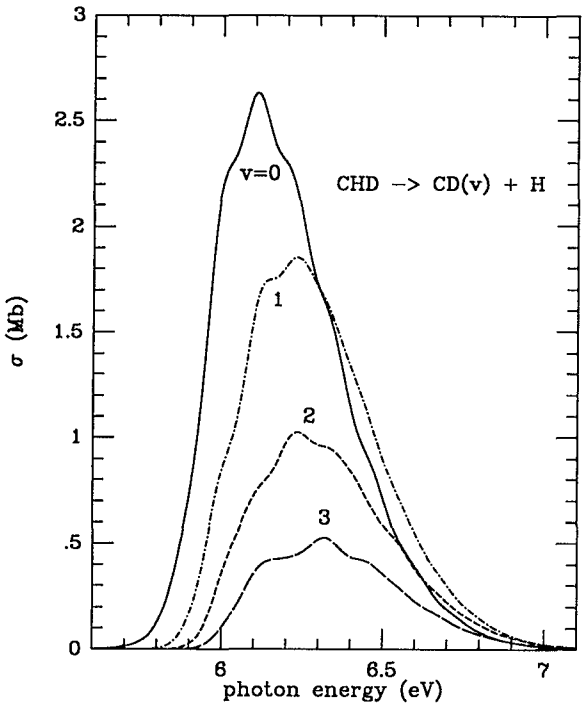

FIG. 16. Partial cross sections (in Mb, 1 Mb$=10^{-18}$ cm^2) for dissociation of CHD into CD+H are plotted as functions of the energy $\hbar\omega$ (in eV) of the exciting radiation for $v=0$–3.

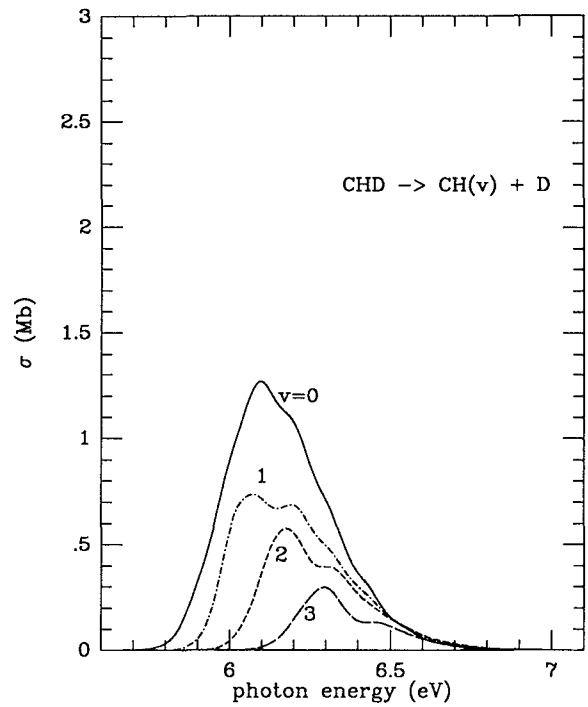

FIG. 17. Partial cross sections (in Mb, 1 Mb$=10^{-18}$ cm^2) for dissociation of CHD into CH+D are plotted as functions of the energy $\hbar\omega$ (in eV) of the exciting radiation for $v=0$–3.

tion time because, according to the reflection principle, both r_1 and r_2 will be small initially. Due to the shape of the potential energy surface, it is necessary for both bond lengths to increase, dissociation becoming possible only for values of either r close to the bond length at the saddle point R_s (2.35 a_0). In CHD, the lighter H atom will move close to R_s (and will dissociate) faster than the heavier D atom in CD_2. Consequently, the CD fragment resulting from CHD will be less hot than that resulting from CD_2 at large total energies. The reverse explanation applies to the vibrational fragment distribution of CH resulting from dissociation of CHD and CH_2 and, as can be seen from Fig. 12, at large total energies the CH fragment resulting from CHD is hotter than that resulting from CH_2 dissociation.

E. Vibrationally excited CHD

As has been mentioned in the Introduction, an important question is how selective photodissociation of CHD is. If we define dissociation of CHD to be selective if the branching ratio CD/CH$\geqslant$10, we find that selective photodissociation is only possible at $\hbar\omega < 5.7$ eV or $\hbar\omega > 6.9$ eV. Unfortunately, as can be seen from Fig. 10, there is little intensity at $\hbar\omega < 5.7$ eV in the absorption spectrum. While there is some intensity at $\hbar\omega > 6.9$ eV, this will not be very useful: at these high excitation energies, the $1\,^3A_1 \leftarrow 1\,^3B_1$ spectrum should be strongly overlapped by the coupled $1\,^3A_2/2\,^3B_1 \leftarrow 1\,^3B_1$ spectrum, because the vertical excitation energy for the latter transition is only 7.34 eV.[4] To check whether higher selectively can be achieved using vibrationally mediated photodissociation, we have also performed calculations in which either the CH stretch or the CD stretch were initially excited with one quantum.

In Fig. 18, total photodissociation cross sections and cross sections σ_{CD} and σ_{CH} are plotted for the (0,0), the (1,0), and the (0,1) state, where the first quantum number is for the CD stretch and the second is for the CH stretch. Similarly, branching ratios are plotted in Fig. 19. For a better comparison, the cross sections and branching ratios are plotted as a function of the total energy E of the molecule rather than of $\hbar\omega$. The frequency or wavelength of the exciting radiation can be obtained for the spectra using the initial vibrational energies of CHD, which are 0.36 eV for the (0,0) state, 0.65 eV for the (1,0) state, and 0.75 eV for the (0,1) state. As can be seen from Figs. 18 and 19, the CD/CH branching ratio is smaller for photodissociation of the (1,0) state than for photodissociation of the ground vibrational state for most total energies, except between $E=6.40$ and 6.52 eV. The ratio is smaller than unity (more CH is produced) for total energies in the range [6.60,7.15] eV. The branching ratio also shows quite interesting behavior for photodissociation of the (0,1) state. Photodissociation of this state is selective at $E<6.2$ eV and $E>6.8$ eV. At $E<6.2$ eV, there is still some intensity in the absorption spectrum. In principle, this can be exploited by performing a two-photon experiment involving an IR laser to excite CHD to the (0,1) state and an UV laser producing radiation which is shifted slightly to the red of the onset of the (0,0) absorption spectrum. Such a scheme has been suggested by Zhang *et al.*[17] for selective photodissociation of HOD. Unfortunately, such an experiment may be difficult to perform. For CH_2, the symmetric stretch

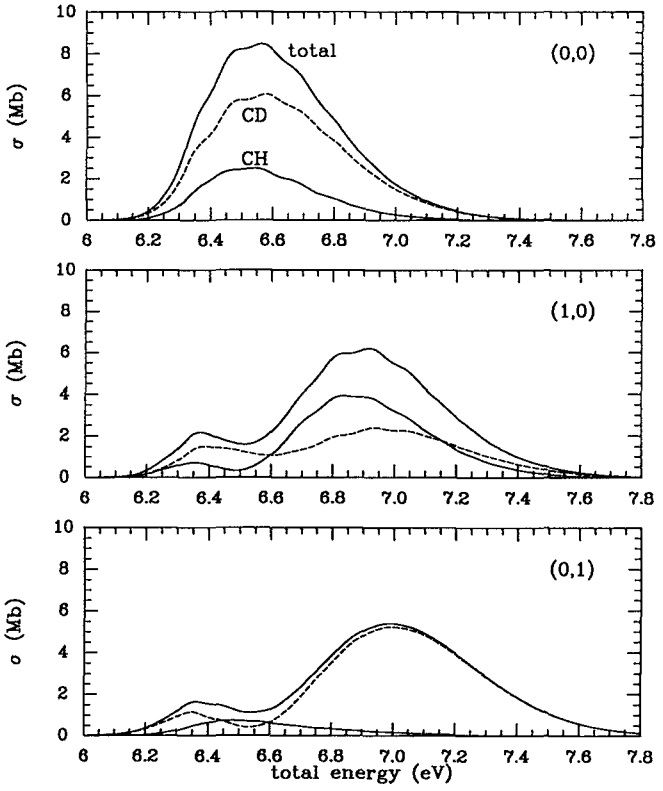

FIG. 18. Total cross sections (upper solid line) and the cross sections σ_{CH} (lower solid line) and σ_{CD} (dashed line) (in Mb, 1 Mb$=10^{-18}$ cm^2) are compared for photodissociation of CHD in three different initial vibrational states, i.e., the (0,0), (1,0), and (0,1) states. Here, the first quantum number is for the CD stretch, and the second for the CH stretch vibration. The cross sections are plotted as a function of the total energy E of the molecule. For conversion of E to $\hbar\omega$, see Sec. IV E.

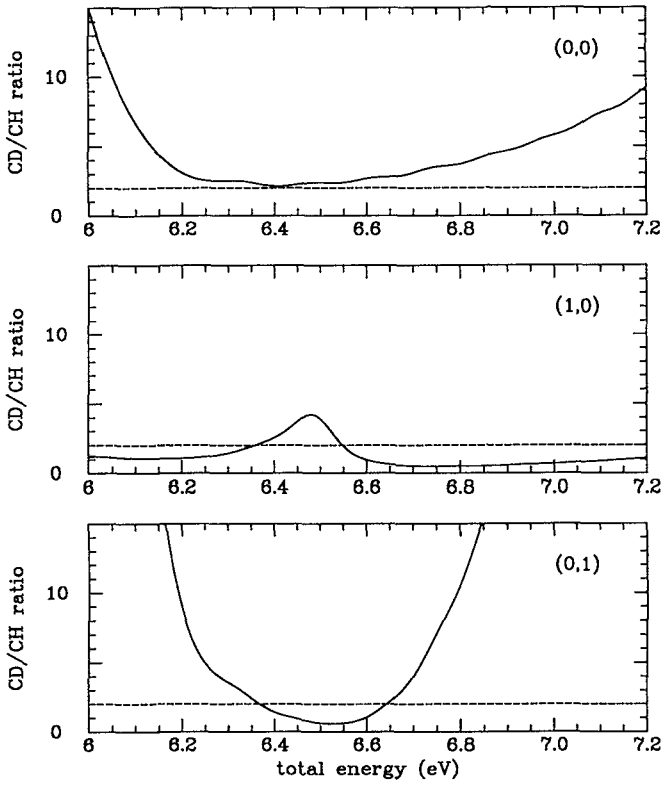

FIG. 19. The CD/CH branching ratios are compared for photodissociation of CHD in three different initial vibrational states, i.e, the (0,0), (1,0), and (0,1) states. Here, the first quantum number is for the CD stretch, and the second for the CH stretch vibration. The cross sections are plotted as a function of the total energy E of the molecule. For conversion of E to $\hbar\omega$, see Sec. IV E.

and antisymmetric stretch transition moments are quite small,[44] and the same should be true for the CH and CD stretch modes of CHD. The spectral range at the red side of the spectrum over which photodissociation is selective and over which the absorption intensity is reasonable should further increase with increased excitation of the CH stretch.[17]

Note that photodissociation of (0,1) CHD is also selective at $E>6.8$ eV where there is considerable intensity in the absorption spectrum. Unfortunately, it may be hard to exploit this selectivity in vibrationally mediated photodissociation: the frequency of the UV laser exciting (0,1) CHD at $E\approx 6.8$ eV will also excite (0,0) CHD at $E\approx 6.4$ eV. Therefore, selective vibrationally mediated absorption will only be possible employing a very strong IR laser. Finally, it should be noted that the behavior of the branching ratio in photodissociation of the (0,0), (1,0), and (0,1) states of CHD is quite similar to that of HOD.[16]

We conclude that vibrationally mediated photodissociation of CHD can be both selective and reasonably efficient over only a small region of the spectrum. As has been shown for HOD, in principle photodissociation can be made selective over the entire range of the spectrum if a more active scheme of control is used: such a scheme would involve an intensive IR laser together with a UV laser which gives an ultrashort pulse ($t\approx 5$ fs) once the molecule prepared in a nonstationary state by the IR laser has a convenient position and/or momentum distribution.[45] At present, such an experiment is not possible because the ultrashort laser pulses in the UV are not available yet. Also, for CHD such an experiment should involve a very intensive IR laser, because of the problem of the low transition moments already mentioned.[44]

V. CONCLUSIONS

We have calculated quantitative total and partial (vibrationally resolved) cross sections for photodissociation of vibrationless CH_2 ($\tilde{X}\,^3B_1$) and its isotopomers CD_2 and CHD through the first excited triplet ($1\,^3A_1$) state. Vibrationally mediated photodissociation of CH_2 and CHD have also been investigated. A two-dimensional wave packet method which employs the LHL approximation was used. In the calculations, *ab initio* potential energy surfaces and an *ab initio* transition dipole moment function were employed.

The peak positions in both of the calculated CH_2 and CD_2 absorption spectra correspond well with the positions of unassigned peaks in the mass resolved 3+1 REMPI spectra of Irikura and Hudgens,[23] provided that these

peaks are due to two-photon transitions rather than three-photon transitions. Perhaps the mass selective 2+1 REMPI experiment[41] can be extended to larger wavelengths, allowing a more definite assignment of these peaks.

The trends found in photodissociation of vibrationless and vibrationally excited CH_2 are very similar to those found previously in photodissociation of water.[7] Both the $v_s'', v_a'' = (0,0)$ and (1,0) spectra show diffuse structure, which is not present in the (0,1) spectrum. The overall shape of the (0,0) and (1,0) spectra and the positions of the features appearing in these spectra are in good agreement with predictions of a two-dimensional Franck–Condon model.[39,40] Photodissociation of (0,1) CH_2 produces CH fragments which are much colder than those resulting from photodissociation of (0,0) and (1,0) CH_2.

The CD_2 absorption spectrum is somewhat narrower than the CH_2 spectrum, and has a larger maximum, which is shifted slightly to the blue when compared to CH_2. In all these aspects (narrowness, maximum value, blue shift), the CHD absorption spectrum is intermediate between those of CH_2 and CD_2. The vibrational level distribution of CD produced by dissociating CD_2 is shifted toward higher v when compared to the CH fragment vibrational level distribution produced by dissociation of CH_2. The CD fragment vibrational level distribution resulting from CHD photodissociation is colder than that resulting from dissociation of CD_2, due to the decrease in the interaction time over which vibrational excitation occurs to CHD. Likewise, photodissociation of CHD produces warmer CH fragments than photodissociation of CH_2.

In photodissociation of $v_{CD}'', v_{CH}'' = (0,0)$ CHD, the CD/CH branching ratio is large, reaching a lower limit of two at intermediate excitation energies. Efficient selective vibrational excitation is not possible at either the red or the blue end of the spectrum. On the other hand, vibrationally mediated photodissociation can be both reasonably efficient and selective if the CH stretch is excited with one quant prior to dissociation at the red side of the spectrum. Selective excitation at the blue side of the spectrum would only be feasible employing a very strong IR laser which would leave no molecules present in the vibrational ground state.

In all aspects discussed here, photodissociation of CH_2 through the $1\,^3A_1$ state is very similar to photodissociation of water in the first absorption band.[6] Actually, so far we have only found two differences between these processes. First, in photodissociation of water, the rotational distribution of the OH fragment is almost completely determined by the excitation steps,[6] while the rotational distribution of CH is determined by the final state interaction.[5] For CH_2, this final state interaction is much stronger due to the anisotropy of the potential in the exit channel, which is almost absent in photodissociation of water in the first absorption band. Second, for CH_2 the transition dipole moment function shows a stronger dependence on r_1 and r_2 in the Franck–Condon region than water. Therefore, it is more important to include the full coordinate dependence in the transition dipole moment function when performing dynamics calculations for CH_2 than for water.

ACKNOWLEDGMENTS

This work was supported by the Netherlands Organization for Scientific Research, NWO, and the Netherlands Foundation of Chemical Research, SON.

[1] S. S. Prasad and W. T. Huntress, Jr., Astrophys. J. Suppl. **43**, 1 (1980).
[2] E. F. van Dishoeck and J. H. Black, Astrophys. J. Suppl. **62**, 109 (1986).
[3] J. Römelt, S. D. Peyerimhoff, and R. J. Buenker, Chem. Phys. **54**, 147 (1981).
[4] R. A. Beärda, M. C. van Hemert, and E. F. van Dishoeck, J. Chem. Phys. **97**, 8240 (1992).
[5] G. J. Kroes, E. F. van Dishoeck, R. A. Beärda, and M. C. van Hemert, J. Chem. Phys. **99**, 228 (1993).
[6] V. Engel, V. Staemmler, R. L. VanderWal, F. F. Crim, R. J. Sension, B. Hudson, P. Andresen, S. Hennig, K. Weide, and R. Schinke, J. Phys. Chem. **96**, 3201 (1992).
[7] V. Engel, R. Schinke, and V. Staemmler, J. Chem. Phys. **88**, 129 (1988).
[8] N. E. Henriksen, J. Zhang, and D. G. Imre, J. Chem. Phys. **89**, 5607 (1988).
[9] K. Weide, S. Hennig, and R. Schinke, J. Chem. Phys. **91**, 7630 (1989).
[10] K. Weide and R. Schinke, J. Chem. Phys. **87**, 4627 (1987).
[11] K. Weide and R. Schinke, J. Chem. Phys. **90**, 7150 (1989).
[12] E. Segev and M. Shapiro, J. Chem. Phys. **77**, 5604 (1982).
[13] G. Theodorakopoulos, C. A. Nicolaides, R. J. Buenker, and S. D. Peyerimhoff, Chem. Phys. Lett. **89**, 164 (1982).
[14] M. von Dirke and R. Schinke, Chem. Phys. Lett. **196**, 51 (1992).
[15] G. J. Kroes (unpublished results).
[16] V. Engel and R. Schinke, J. Chem. Phys. **88**, 6831 (1988).
[17] J. Zhang, D. G. Imre, and J. H. Frederick, J. Phys. Chem. **93**, 1840 (1989).
[18] N. Shafer, S. Satyapal, and R. Bersohn, J. Chem. Phys. **90**, 6807 (1989).
[19] R. L. VanderWal, J. L. Scott, and F. F. Crim, J. Chem. Phys. **92**, 803 (1990).
[20] I. Bar, Y. Cohen, D. David, S. Rosenwaks, and J. J. Valentini, J. Chem. Phys. **93**, 2146 (1990).
[21] R. L. VanderWal, J. L. Scott, F. F. Crim, K. Weide, and R. Schinke, J. Chem. Phys. **94**, 3548 (1991).
[22] I. Bar, Y. Cohen, D. David, T. Arusi-Parpar, S. Rosenwaks, and J. J. Valentini, J. Chem. Phys. **95**, 3341 (1991).
[23] K. K. Irikura and J. W. Hudgens, J. Phys. Chem. **96**, 518 (1992).
[24] A. Untch, K. Weide, and R. Schinke, J. Chem. Phys. **95**, 6496 (1991).
[25] K. C. Kulander and E. J. Heller, J. Chem. Phys. **69**, 2439 (1978).
[26] E. J. Heller, J. Chem. Phys. **68**, 2066 (1978).
[27] G. G. Balint-Kurti, R. N. Dixon, and C. C. Marston, J. Chem. Soc. Faraday Trans. **86**, 1741 (1990).
[28] G. G. Balint-Kurti and M. Shapiro, Adv. Chem. Phys. **60**, 403 (1985).
[29] J. Zhang and D. G. Imre, J. Chem. Phys. **90**, 1666 (1989).
[30] G. J. Kroes and M. C. van Hemert, J. Chem. Phys. **100**, 1128 (1994).
[31] R. T. Lawton and M. S. Child, Mol. Phys. **37**, 1799 (1979).
[32] R. T. Lawton and M. S. Child, Mol. Phys. **40**, 773 (1980).
[33] R. Schinke, *Photodissociation Dynamics* (Cambridge University Press, Cambridge, 1993).
[34] R. Heather and H. Metiu, J. Chem. Phys. **86**, 5009 (1987).
[35] G. G. Balint-Kurti, R. N. Dixon, and C. C. Marston, Int. Rev. Phys. Chem. **11**, 317 (1992).
[36] H. Tal-Ezer and R. Kosloff, J. Chem. Phys. **81**, 3967 (1984).
[37] D. Kosloff and R. Kosloff, J. Comp. Phys. **52**, 35 (1983).
[38] P. Jensen and P. R. Bunker, J. Chem. Phys. **89**, 1327 (1988).
[39] M. Braunstein and R. T. Pack, J. Chem. Phys. **96**, 891 (1992).
[40] R. T. Pack, J. Chem. Phys. **65**, 4765 (1976).
[41] K. K. Irikura, R. D. Johnson III, and J. W. Hudgens, J. Phys. Chem. **96**, 6131 (1992).
[42] E. J. Heller, Acc. Chem. Res. **14**, 368 (1981).
[43] J. O. Hirschfelder, C. F. Curtiss, and R. B. Bird, *Molecular Theory of Gases and Liquids* (Wiley, New York, 1954), p. 663.
[44] P. R. Bunker and S.R. Langhoff, J. Mol. Spectrosc. **102**, 204 (1983).
[45] B. Amstrup and N. E. Henriksen, J. Chem. Phys. **97**, 8285 (1992).